タイトル Title	Effect of Film-Forming Additive in Ionic Liquid Electrolyte on Electrochemical Performance of Si Negative-Electrode for LIBs
著者 Auther(s)	Yamaguchi, Kazuki; Domi, Yasuhiro; Usui, Hiroyuki; Shimizu, Masahiro; Morishita, Shota; Yodoya, Shuhei; Sakata, Takuma; Sakaguchi, Hiroki
掲載誌・巻号・ページ Citation	Journal of the Electrochemical Society , 166 (2) : A268 - A276
刊行日 Issue Date	2019-01-28
資源タイプ Resource Type	学術雑誌論文 / Journal Article
版区分 Resource Version	出版社版 / Publisher
権利 Rights	© The Author(s) 2019. Published by ECS. This is an open access article distributed under the terms of the Creative Commons Attribution 4.0 License (CC BY, http://creativecommons.org/licenses/by/4.0/), which permits unrestricted reuse of the work in any medium, provided the original work is properly cited.
DOI	10.1149/2.0971902jes
URL	http://repository.lib.tottori-u.ac.jp/6423

Effect of Film-Forming Additive in Ionic Liquid Electrolyte on Electrochemical Performance of Si Negative-Electrode for LIBs

Kazuki Yamaguchi,[1,2] Yasuhiro Domi,[1,2,*] Hiroyuki Usui,[1,2] Masahiro Shimizu,[1,2,*] Shota Morishita,[1,2] Shuhei Yodoya,[2,3] Takuma Sakata,[1,2] and Hiroki Sakaguchi[1,2,*,z]

[1] *Department of Chemistry and Biotechnology, Graduate School of Engineering, Tottori University, Koyama-cho, Tottori 680-8552, Japan*
[2] *Center for Research on Green Sustainable Chemistry Tottori University, Koyama-cho, Tottori 680-8552, Japan*
[3] *Course of Chemistry and Biotechnology, Department of Engineering, Graduate School of Sustainability Science, Tottori University, Koyama-cho, Tottori 680-8552, Japan*

1-ethyl-3-methylimidazolium bis(trifluoromethanesulfonyl)amide (EMI-TFSA) is one of the promising ionic liquids as electrolyte solvent to enhance the electrochemical performance of Si electrode for Li-ion batteries (LIBs) because of its low viscosity and high conductivity. However, it has low stability against reduction and its reductive decomposition product inhibits Li^+ insertion to electrodes, leading to poor cycling stability. To exert a potential of EMI-TFSA, we employed vinylene carbonate (VC) as film-forming additive. Si electrode exhibited very high cycling stability and rate capability in 20 vol.% VC-added EMI-TFSA-based electrolyte. In addition, by replacing TFSA anion with bis(fluorosulfonyl)amide (FSA) for Li salt and ionic liquid solvent, an excellent cycling performance and outstanding rate capability was achieved. VC cannot only fabricate a good surface film but also lower the interaction between Li^+ and FSA^-, providing smooth desolvation of FSA^- to obtain better high-rate performance. Non-flammability of the VC-added electrolytes was confirmed by fire resistance test in closed-system: no ignition was observed even at 300°C. Consequently, we found that mixture electrolyte consisted of EMI-based ionic liquid and VC, especially 1 M LiFSA/EMI-FSA with 20 vol.% VC, is a prospective candidate for simultaneously enhancing the electrochemical performance of Si electrode as well as safety of LIBs.
 [DOI: 10.1149/2.0971902jes]

Manuscript submitted November 21, 2018; revised manuscript received January 11, 2019. Published January 28, 2019.

Li-ion batteries (LIBs) have been applied as power sources of not only portable electronic devices but also electric vehicles (EVs). To further increase in cruising distance of EVs per charge, positive and negative electrode materials with high capacity have been required. Silicon (Si) has attracted much attention as an active material of negative electrode for next-generation LIBs because of its high theoretical capacity of 3600 mA h g^{-1} ($Li_{15}Si_4$), which is ten times as high as capacity of graphite negative electrode used in current LIBs.[1] However, Si suffers from a severe stress generated by its extreme volumetric changes during alloying-dealloying reaction. Accumulation of a strain due to the stress results in disintegration of active material layer. In addition, Si has several drawbacks such as low electrical conductivity and slow Li^+ diffusion.[2,3] Hence, Si shows only poor cycling stability. To improve the stability, we have developed composite electrode consisted of Si and other material which can compensate the drawbacks.[4–7]

Electrolytes are one of the key components, which determine lifetimes and safety of LIBs. While a carbonate-based organic electrolyte has been used in commercial LIBs, the electrolyte is not necessarily the best for the Si-based electrode because Si volume extremely changes during charge-discharge reaction unlike graphite. In addition, safety assurance has been required more than ever with an increase in size and energy density of batteries. Since the carbonate-based electrolyte is volatile and flammable, it can trigger ignition and explosion of batteries when accident like internal short-circuit happens. Therefore, an electrolyte used in LIBs for EVs demands non-flammability. Ionic liquids are highly potential candidate as non-flammable electrolyte, because they have a negligible vapor pressure, non-flammability, and a wide electrochemical window.[8–11] We have focused on ionic liquids as electrolyte solvents, and investigated their applicability to Si-based negative electrodes.[6,12–15] As a result, we have found that a cycling stability of Si-based electrodes significantly improve in some ionic liquid electrolytes compared to that in conventional organic electrolytes.[6,14,15] However, the high viscosity of quaternary ammonium-based ionic liquid electrolytes, such as piperidinium and pyrrolidinium-based, hinders charge transfer reaction at electrode-electrolyte interface, leading to deteriorating cycle life and rate performance of Si electrode. In contrast, imidazolium-based ionic liquids have lower viscosity and higher conductivity than quaternary ammonium-based ionic liquids.[12,16–18] For example, viscosity and conductivity of 1-ethyl-3-methylimidazolium bis(trifluoromethanesulfonyl)amide (EMI-TFSA) is 33 mPa s and 8.3 mS cm^{-1} at 298 K, whereas those of 1-methyl-1-propylpyrrolidinium bis(trifluoromethanesulfonyl)amide (Py13-TFSA) is 61 mPa s and 3.9 mS cm^{-1} at 298 K, respectively.[18] Hence, the EMI-based ionic liquids may enhance the battery performance. Nevertheless, EMI cation is easily decomposed reductively and the decomposition product inhibits Li^+ insertion into the electrode.[12,19,20] This is one of the reasons for hindrance of application of EMI-based ionic liquids to electrolytes for LIBs.

It is well known that film-forming additives, such as vinylene carbonate (VC) and fluoroethylene carbonate (FEC), can suppress continual electrolyte decomposition because they preferentially decompose to form stable surface film on the electrode.[21–26] Sun et al. reported that reversible charge-discharge reaction of graphite electrode proceeded in pyrrolidinium and piperidinium-based ionic liquid electrolytes by addition of VC.[27] Ishikawa et al. applied 0.8 mol dm^{-3} (M) LiTFSA/1-ethyl-3-methylimidazolium bis(fluorosulfonyl)amide (EMI-FSA) with 10 wt% propylene carbonate (PC) and VC to graphite electrode, and confirmed that Li^+ insertion/extraction reaction occurred in the presence of VC.[28] If a favorable film derived from additives is also formed on the Si electrode surface in the EMI-based ionic liquid electrolytes, reductive decomposition of EMI cation will be suppressed to achieve a high rate capability. On the other hand, FSA anion enables a reversible charge-discharge reaction of graphite or Si electrode in EMI-based ionic liquid electrolyte without organic additives. Ishikawa et al. reported that a discharge capacity of Si–Ni–carbon composite electrode was 932.5 mA h g^{-1} even at the 20th cycle in 0.3 mol kg^{-1} LiTFSA/EMI-FSA, whereas no capacity was obtained in LiTFSA/EMI-TFSA.[20] They considered that such excellent performance with FSA-based electrolyte correlates with very low interfacial and charge–transfer resistances at the Si-based composite negative electrode. Piper et al. applied 1.2 M LiFSA/EMI-FSA to cyclized-polyacrylonitrile-based Si nanocomposite architecture (nSi-cPAN), and demonstrated that the nSi-cPAN electrode maintained a discharge capacity of more than 2000 mA h g^{-1} after 100 cycles.[29]

*Electrochemical Society Member.
[z]E-mail: sakaguch@chem.tottori-u.ac.jp

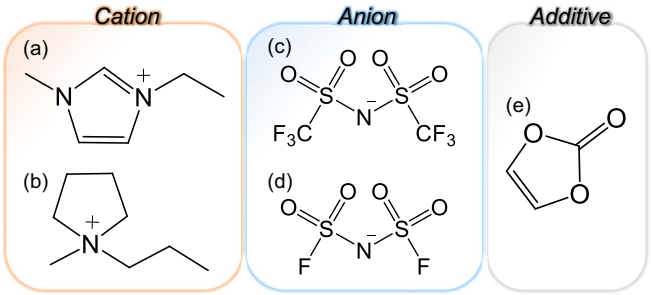

Figure 1. Chemical structure of (a) 1-ethyl-3-methylimidazolium (EMI^+), (b) 1-methyl-1-propylpyrrolidinium ($Py13^+$), (c) bis(trifluoromethanesulfonyl)amide ($TFSA^-$), (d) bis(fluorosulfonyl)amide (FSA^-), and (e) vinylene carbonate (VC).

However, influence of EMI-FSA on the cycling performance of Si-alone electrode is not sufficiently understood because these electrodes were fabricated by mixing active materials with binders and conductive additives. They causes side reaction, which makes difficult to observe reaction of Si itself.

We have applied a gas-deposition method to prepare electrode, which requires no binders and conductive additives.[30] Thus, this method is suitable for analyzing the reaction behavior at interface between active materials and electrolytes. In this study, we investigated an effect of VC-addition to EMI-based ionic liquid electrolytes on a cycling performance of Si-alone negative electrode for LIBs. We also studied relationship between cation/anion structure in ionic liquid electrolyte and electrochemical performance of Si electrode. Coordination environment of Li^+ in each electrolyte was explored by Raman spectroscopic measurements. To confirm non-flammability of VC-added ionic liquid electrolyte, fire-resistance test was also conducted.

Experimental

Preparation and characterization of electrolyte.—We used two types of commercially available ionic liquids: the one is EMI-TFSA (Kanto Chemical Co., Inc.) and the other is EMI-FSA (Kanto Chemical Co., Inc.). Chemical structures of these ionic liquids were shown in Figure 1. The electrolytes were 1 M LiTFSA (99.9%, Kishida Chemical Co., Ltd.) dissolved in EMI-TFSA and 1 M lithium bis(fluorosulfonyl)amide (LiFSA; 99%, Kishida Chemical Co., Ltd.) dissolved in EMI-FSA. The anion of the Li salt was the same as that of the ionic liquid: only single anion species was in the electrolytes. Then, 5 or 20 vol.% of VC (Kishida Chemical Co., Ltd.) was added to each electrolyte. The ionic conductivity was investigated by an electrochemical impedance spectroscopy (EIS) with CompactStat of Ivium Technologies using the cell with two Pt electrodes under argon atmosphere at various temperatures from 298 to 333 K. To confirm the superiority of EMI-based electrolyte, we also adopted an electrolyte consisted of Py13-TFSA (Kanto Chemical Co., Inc.) which has high stability against oxidation/reduction.

The interactions between Li^+ and VC or FSA anion of ionic liquid electrolytes were analyzed by using a Raman microscopy system (NanofinderFLEX, Tokyo Instruments, Inc.) with 532 nm line of Nd:YAG laser through a 50-power objective lens at room temperature. Although the electrolytes used in this study were consisted of mainly ionic liquids, VC, that is organic film-forming additive was also contained; hence, advantage of non-flammability might be lost. Thus, we conducted fire-resistance tests by using a flash point tester (Setaflash Series: 33000-0, STANHOPE SETA LTD.). These tests were performed in line with rapid equilibrium closed cup method according to International Organization for Standardization (ISO) 3679:2004 and Japanese Industrial Standards (JIS) K2265-2. We have introduced this technique as the evaluation method for the flame retardancy of ionic liquid electrolytes for the first time.[31,32] Detail condition and procedure have been described in previous our report.[31]

Cell assembly and electrochemical measurements.—Si electrodes were prepared by a gas-deposition (GD) method using commercially available Si powder (FUJIFILM Wako Pure Chemical Corporation, 99.9%, average particle size: 20 μm). The detail condition is listed in the previous papers.[14,33] The deposited weight of active material on the Cu substrate was measured to an accuracy of 1 μg with an XP6 ultramicrobalance (Mettler-Toledo) equipped with an anti-vibration table. Si electrodes in the range of 28−32 μg were adopted. We confirmed that the GD-electrode was composed only of Si by XRD pattern (Figure 2a) and that Si was crystalline by Raman spectrum (Figure 2b). Figure 2c and 2d shows surface and cross-sectional field-emission scanning electron microscopic (FE-SEM) image of the electrode. The thickness and area of active material layer were approximately 1.6 μm and 0.8 cm^2, respectively. We fabricated 2032-type coin cells, which contain Si electrode as working electrode, Li metal foil (Rare Metallic, 99.90%, thickness: 1.0 mm) as counter electrode, ionic liquid electrolyte, and glass-fiber filter as a separator. We performed the charge–discharge test of the cells by using an electrochemical measurement system (HJ-1001 SM8 and HJ-1001 SD8, Hokuto Denko Co., Ltd) in the potential range between 0.005 and 2.000 V vs. Li^+/Li at 303 K under a current density of 420 mA g^{-1} (0.12 *C*). Rate capability was also evaluated under current density range from 1050 to 4200 mA g^{-1} (0.29–1.2 *C*). EIS analysis using a three-electrode type cell was performed at 0.005 V vs. Li^+/Li in the frequency range of 100 kHz to 10 mHz with an amplitude of 5 mV at 303 K. The surface morphology of the electrodes before and after cycling was observed by FE-SEM (JSM-6701F; JEOL Ltd.).

Results and Discussion

Electrochemical performance in an electrolyte consisted of EMI-TFSA.—Figure 3a shows charge-discharge profiles of Si electrodes at the first cycle in an electrolyte of 1 M LiTFSA/EMI-TFSA without and with 5 or 20 vol.% VC. Figure 3b also shows corresponding differential charge capacity versus potential (d*Q*/d*V*) profiles. In all electrolytes, potential plateaus appeared at 0.1 and 0.4 V vs. Li^+/Li on charge and discharge curves, respectively. These plateaus indicate that lithiation/delithiation reactions of Si proceeded with or without VC. However, a potential gradient (Figure 3a) and a broad peak (Figure 3b) was observed from 0.6 to 0.2 V vs. Li^+/Li in additive free electrolyte, which is attributed to reductive decomposition of EMI cation. Although a charge capacity was 5730 mA h g^{-1} in additive free electrolyte, a discharge capacity was only 2700 mA h g^{-1}, resulting in low Coulombic efficiency of 47%. In contrast, no potential gradient and broad peak at 0.6 V vs. Li^+/Li was confirmed in the electrolyte with VC. In VC-added electrolytes, irreversible capacity reduced and therefore the Coulombic efficiency improved (VC 5 vol.%: 81% and 20 vol.%: 66%). From these results, it is found that reductive decomposition of EMI cation is suppressed in the presence of VC. Figure 3c shows cycling performances of Si electrode in 1 M LiTFSA/EMI-TFSA without and with VC. The Si electrode exhibited a relatively high discharge capacity at initial cycles in additive free electrolyte, though most of its capacity was lost at only 10 cycles. This is because surface film derived from EMI cation was formed on Si electrode surface, which prohibits Li^+ insertion into Si active material layer.[12,20] On the other hand, a rapid capacity decay until initial 10 cycles was suppressed by adding VC 5 vol.%. Nevertheless, the capacity started to decrease after 50 cycles and almost no capacity was obtained after 100 cycles.

To confirm the reason for capacity degradation after 50 cycles, we observed the surface morphology of Si electrode after the 40th and 70th cycles by FE-SEM (Figure 4a and 4b). Although the capacity quite decreased at the 70th cycle, the degree of electrode disintegration was comparable with the electrode at the 40th cycle before starting capacity decay. Thus, the main reason for capacity degradation after 50 cycles was not electrode disintegration. We considered mechanism of

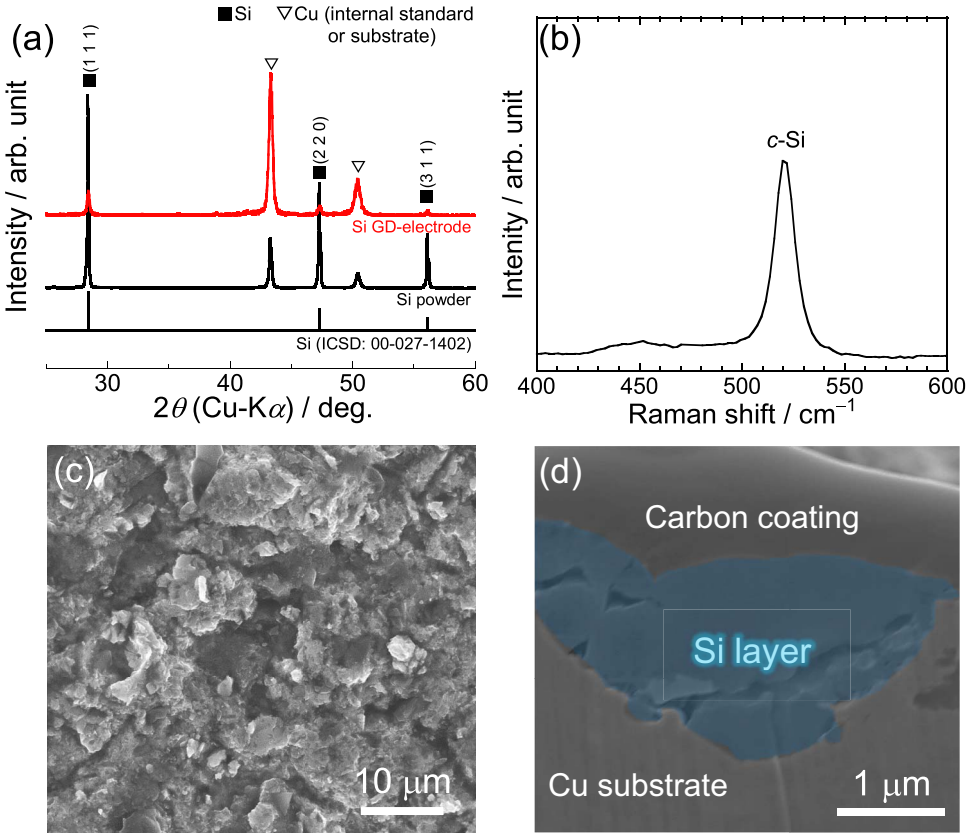

Figure 2. (a) XRD patterns and Si powder and Si GD-electrode as prepared. (b) Raman spectrum of Si GD-electrode. (c) Surface and (d) cross-sectional FE-SEM image of Si GD-electrode as prepared. The electrode surface was coated with carbon to protect it against damage by the Ga^+ beam of focused ion beam.

capacity decay as follows. A volume of Si expands up to 380% when Si reacts with Li to form $Li_{15}Si_4$, and repeating volumetric change during charge-discharge cycling damages a surface film on the Si electrode. While VC is decomposed at newly exposed electrode surface, 5 vol.% might be almost consumed during repeating several tens cycle. As a result, EMI cation eventually is reductively decomposed and passivation of negative electrode proceeds. Hence, 5 vol.% VC was insufficient to form stable surface film for long term cycling and the discharge capacity started to decay at around 50th cycle (Figure 3c). To address this issue, we furthermore added VC (total 20 vol.%) to EMI-based electrolyte. A discharge capacity gradually increased in this electrolyte at initial cycles. This is possibly due to activation process of Si electrode. In contrast to 5 vol.% VC, the electrode achieved a high cycling stability with a discharge capacity of 1500 mA h g^{-1} after 200 cycles. This is because VC-derived surface film is formed on the electrode in the presence of sufficient amount of VC, and it suppresses reductive decomposition of EMI cation over 200 cycles. EIS measurement was conducted to reveal the reason for suppression of capacity decay in the VC-added electrolyte. Figure 4c displays Nyquist plot of Si electrode charged at 0.005 V vs. Li^+/Li after the 1st and 40th cycles. In additive free electrolyte, interfacial resistance of Si electrode at the 40th cycle became approximately four-fold compared to that at the 1st cycle. This suggests Li^+ insertion into Si electrode is hardly to occur at the 40th cycle due to the decomposition of EMI cation. On the other hand, the resistance was significantly low at the 1st cycle in the 20 vol.% VC-added electrolyte and exhibited almost no change at

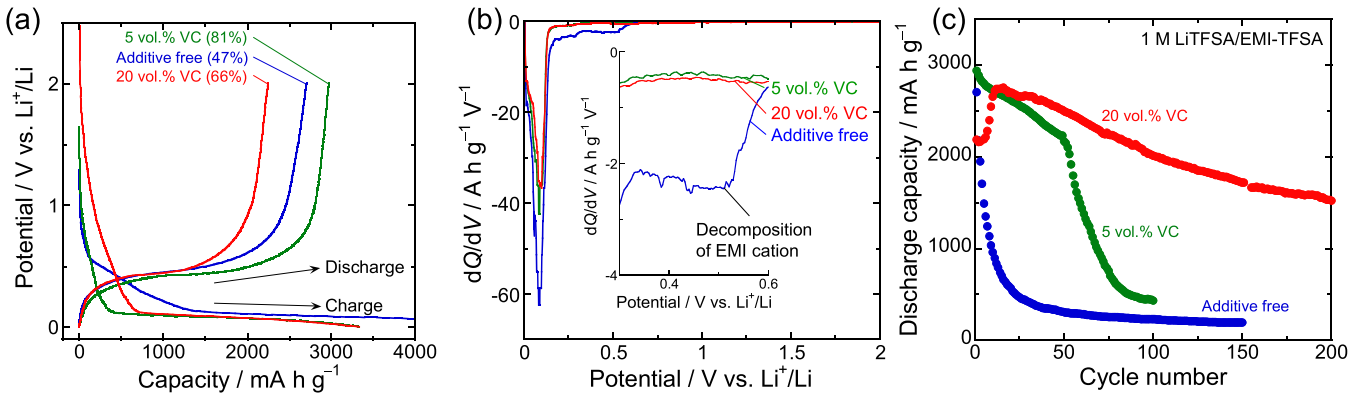

Figure 3. (a) Charge-discharge (Li-insertion/extraction) property, (b) differential capacity vs. voltage (dQ/dV) curves, and (c) cycling performance of Si electrode in 1 M LiTFSA/EMI-TFSA without and with 5 vol.% or 20 vol.% VC. The initial charge capacity obtained in the 1 M LiTFSA/EMI-TFSA without additive was 5730 mA h g^{-1}.

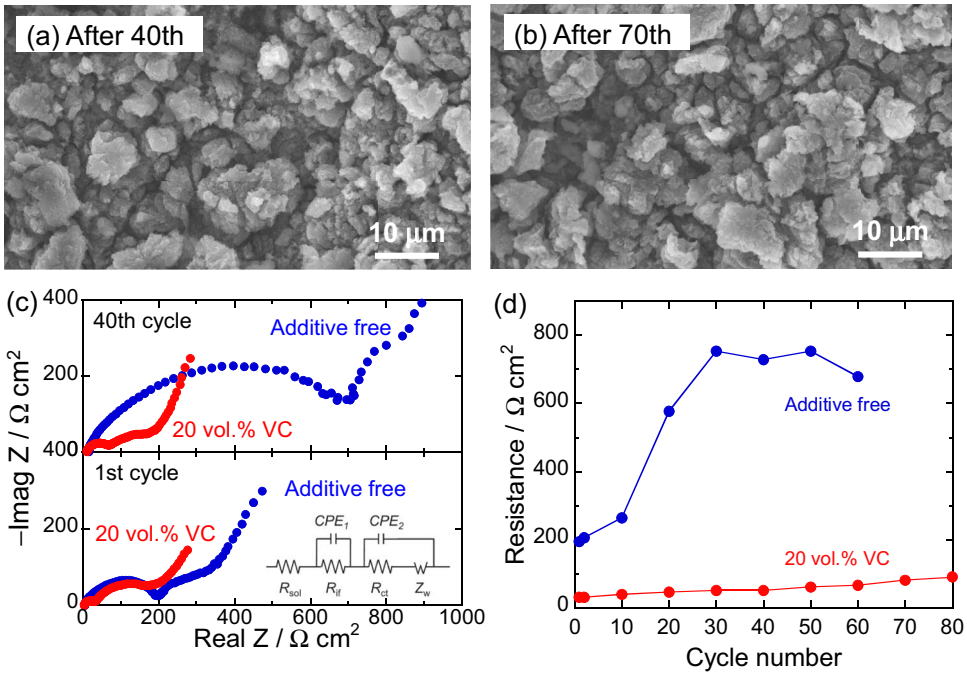

Figure 4. FE-SEM images of Si electrodes after (a) 40 and (b) 70 charge−discharge cycles in 1 M LiTFSA/EMI-TFSA with 5 vol.% VC. (c) Nyquist plots of cell including the electrode charged at 0.005 V in the first cycle. Inset: Randles circuit used in this study for analysis of cell impedance. (d) Change in interfacial resistance of Si electrode versus cycle number in 1 M LiTFSA/EMI-TFSA with and without 20 vol.% VC.

the 40th cycle. Figure 4d shows change in the interfacial resistance of Si electrode versus cycle number in the electrolyte without/with 20 vol.% VC. The resistance increased quickly in first 20 cycles in the additive free electrolyte, whereas it mildly increased until the 80th cycle in the VC-added electrolyte. This means Li^+ can smoothly migrate at the electrode/electrolyte interface. Consequently, VC-derived surface film can suppress the decomposition of EMI cation to maintain low resistance, leading to better cycling performance.

As advantage of EMI-TFSA, they have lower viscosity and higher conductivity than pyrrolidinium-based ionic liquid electrolytes, such as Py13-TFSA. Thus, it is expected that Si electrode in EMI-TFSA exhibits superior rate capability to that in Py13-TFSA.[12] Figure 5 shows rate capability of Si electrode in the TFSA-based electrolyte. Despite our expectation, poor rate capability was observed in 1 M LiTFSA/EMI-TFSA due to decomposition product of EMI cation. A relatively high discharge capacity of 2300 mA h g^{-1} was obtained at a low current density of 0.29 *C* (1050 mA g^{-1}) in 1 M LiTFSA/Py13-TFSA. However, the electrode exhibited only 590 mA h g^{-1} at 1.2 *C* (4200 mA g^{-1}) due to low conductivity of the Py13-based electrolyte (Table I). In contrast, the rate capability of Si electrode was obviously improved in 20 vol.% VC-added electrolytes. This should be attributed to not only increase in the conductivity of electrolyte as shown in Table I but also formation of VC-derived surface film on the electrode to suppress continuous decomposition of the electrolytes. The best rate capability was achieved in 1 M LiTFSA/EMI-TFSA with 20 vol.% VC: a high capacity of 1500 mA h g^{-1} was maintained even at 1.2 *C*. As a consequence, it is clear that VC addition is effective to get potential out of EMI-TFSA.

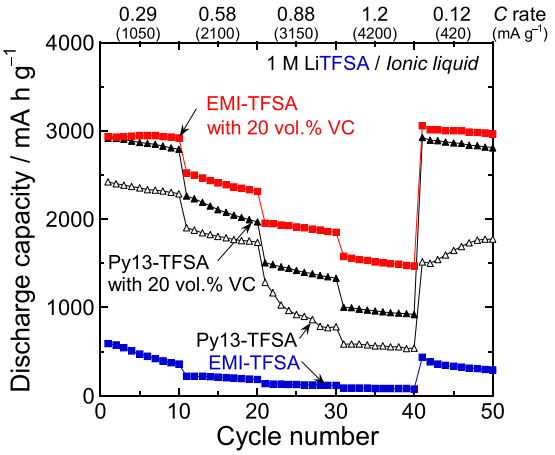

Figure 5. Rate performance of Si electrodes in 1 M LiTFSA/EMI-TFSA and 1 M LiTFSA/Py13-TFSA with/without 20 vol.% VC.

Electrochemical performance in an electrolyte consisted of EMI-FSA.—We also investigated the anion effect of EMI-based electrolyte on cycling performance of Si electrode. Figure 6a shows charge-discharge profiles of Si electrodes at the first cycle in an electrolyte of 1 M LiFSA/EMI-FSA without and with 20 vol.% VC. Figure 6b shows corresponding d*Q*/d*V* profiles. As with TFSA-based electrolytes, potential plateaus were observed at 0.1 V on charge curve and 0.4 V on discharge curve, respectively. However, a broad peak at 0.6 V did not appear even in additive free electrolyte and a new potential gradient appeared at around 1.5 V on charge curve. This is attributed to decomposition of FSA anion.[15] Thus, the FSA-derived surface film was preferentially formed on the electrode to probably suppress reductive decomposition of EMI cation. Coulombic efficiency in the

Table I. Conductivity of EMI- and Py13-based electrolytes without and with VC at 303 K.

Electrolytes	Conductivity / mS cm^{-1}	
	Without VC	With 20 vol.% VC
1 M LiTFSA/Py13-TFSA	1.2	6.1
1 M LiTFSA/EMI-TFSA	4.9	10.5
1 M LiFSA/EMI-FSA	12.3	18.8

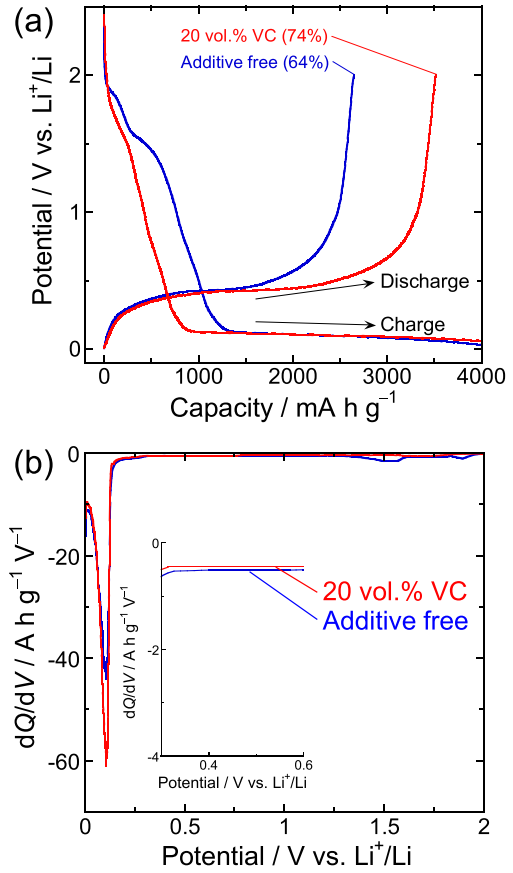

Figure 6. (a) Charge-discharge (Li-insertion/extraction) property of Si electrode in 1 M LiFSA/EMI-FSA without and with 20 vol.% VC. The initial charge capacity obtained in the 1 M LiFSA/EMI-FSA without and with 20 vol.% VC was 4250 and 4740 mA h g^{-1}, respectively. (b) Differential capacity vs. voltage (d*Q*/d*V*) curves of the electrodes in the respective ionic liquid electrolytes. Inset: enlarged view of the curves.

1 M LiFSA/EMI-FSA (64%) was higher than that in 1 M LiTFSA/EMI-TFSA (47%). The efficiency further increased to 74% by 20 vol.% VC addition. This result suggests that VC adding to FSA-based electrolyte is also effective to improve a reversibility of charge-discharge reaction.

Figure 7 shows long-term cycling performance of Si electrode in 1 M LiFSA/EMI-FSA without and with 20 vol.% VC. The electrode

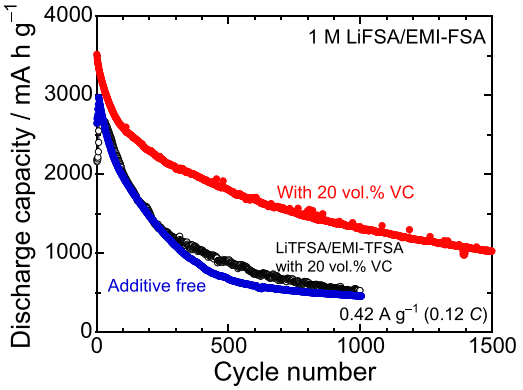

Figure 7. Long-term cycling performance of Si electrode in 1 M LiFSA/EMI-FSA without and with 20 vol.% VC at current density of 420 mA g^{-1} (0.12 *C*). Black open circle corresponds the performance in 1 M LiTFSA/EMI-TFSA with 20 vol.%.

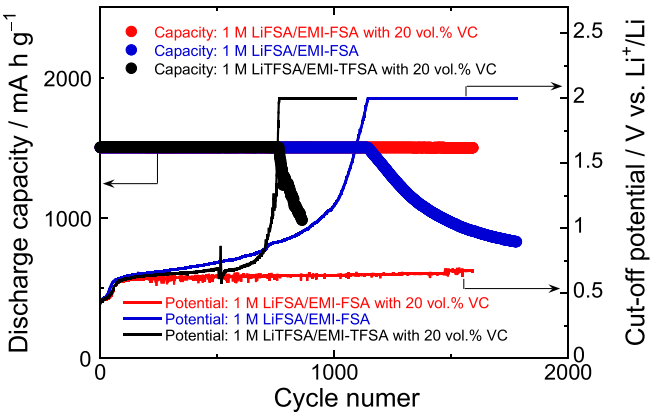

Figure 8. Variation in discharge capacity and discharge cutoff potential of Si electrode versus cycle number in 1 M LiFSA/EMI-FSA without and with 20 vol.% VC at current density of 420 mA g^{-1} (0.12 *C*) under discharge (Li-extraction) capacity limit of 1500 mA h g^{-1}.

maintained a discharge capacity of 500 mA h g^{-1} after 1000 cycles even in additive free electrolyte. This performance was comparable with that in 1 M LiTFSA/EMI-TFSA with 20 vol.% VC, indicating that FSA-derived surface film acts as a protective film suppressing reduction of EMI cation. Surprisingly, much higher cycling stability was obtained in 1 M LiFSA/EMI-FSA with 20 vol.% VC: the Si electrode maintained a high discharge capacity of more than 1000 mA h g^{-1} over 1500 cycles. This excellent performance was probably attributed to composition of surface film on the Si electrode. As well known, decomposition product of FSA anion is LiF, Li_2O, Li_2SO_4, $LiNSO_2$ and so on.[29,34] LiF and Li_2O have extremely high thermodynamic stability, which are good component for surface film to enhance its structural stability.[29] In addition, FSA-derived surface film is relatively thin and homogeneous.[34–36] On the other hand, VC-derived surface film is composed of mainly poly(VC), Li_2CO_3, $Li_2C_2O_4$ etc.[25,37–40] Poly(VC) is insoluble polymer to be useful for fabrication of stable surface film during charge-discharge cycling. Michan et al. suggested that poly(VC) would likely aid surface film elasticity helping to solve the problem of uncontrolled surface-film growth and cracking in the surface film due to the large volumetric change of the Si active materials.[38] Combination of these components possibly makes more stable surface film for long-term cycling to inhibit electrolyte decomposition.

We have demonstrated that a cycle life of a Si-based electrode can be prolonged by moderately controlling the amount of Li insertion–extraction.[6,15,33,41,42] To clarify the merit of using EMI-based electrolyte, a cycle life of Si-alone electrode (Figure 8) was investigated under Li extraction capacity limited to 1500 mA h g^{-1} which is approximately four times higher than graphite electrode. Cycle lives of Si electrodes were 780 and 1150 cycles in 1 M LiTFSA/EMI-TFSA with 20 vol.% VC and 1 M LiFSA/EMI-FSA, respectively. Cycling stability without capacity limit in 1 M LiFSA/EMI-FSA was comparable to that in 1 M LiTFSA/EMI-TFSA with 20 vol.% VC, as shown in Figure 7. On the other hand, the cycle life in 1 M LiFSA/EMI-FSA was obtained 1.5 times as long as that in VC-added TFSA-based electrolyte under capacity limit of 1500 mA h g^{-1}. This result suggests that the FSA-derived surface film rather than the VC-derived one effectively contributes to improving cycle life of Si electrode if change in the volume of Si was moderately suppressed. Since the VC-derived film is tolerant to change in the volume of Si active materials, controlling Li-extraction amount might be less effective to improve the cycle life. In 1 M LiFSA/EMI-FSA with 20 vol.% VC, an excellent cycle life was attained with a reversible capacity of 1500 mA h g^{-1} beyond at least 1600 cycles. In this measurement also, cutoff potential was set between 0.005–2.0 V vs. Li^+/Li. However, a discharge cutoff potential is stopped on the way if the discharge capacity comes at 1500 mA h g^{-1}. It reaches upper limit of 2.0 V when the capacity of

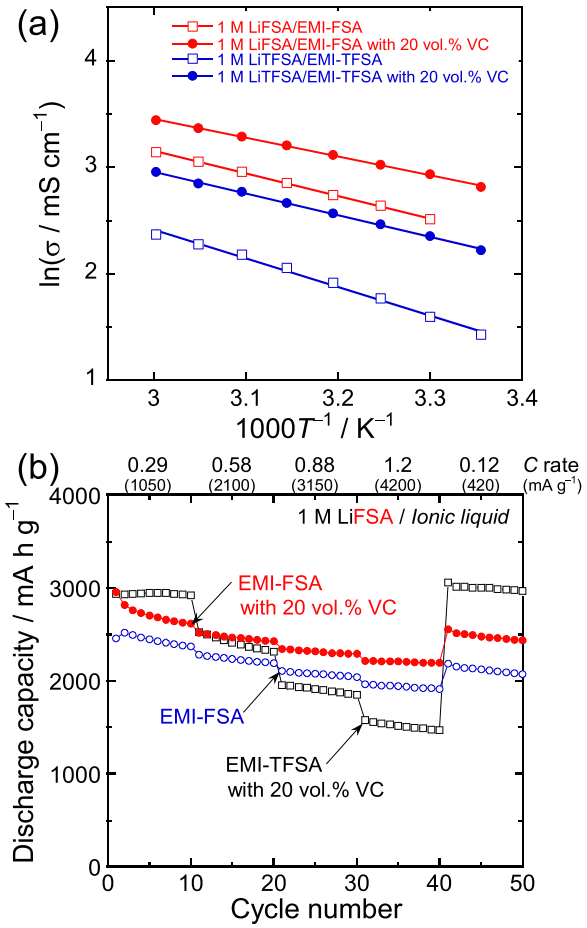

Figure 9. (a) Temperature dependence of ionic conductivity of ionic liquid electrolytes with and without 20 vol.% VC. (b) Rate performance of Si electrodes in 1 M LiFSA/EMI-FSA with and without 20 vol.% VC.

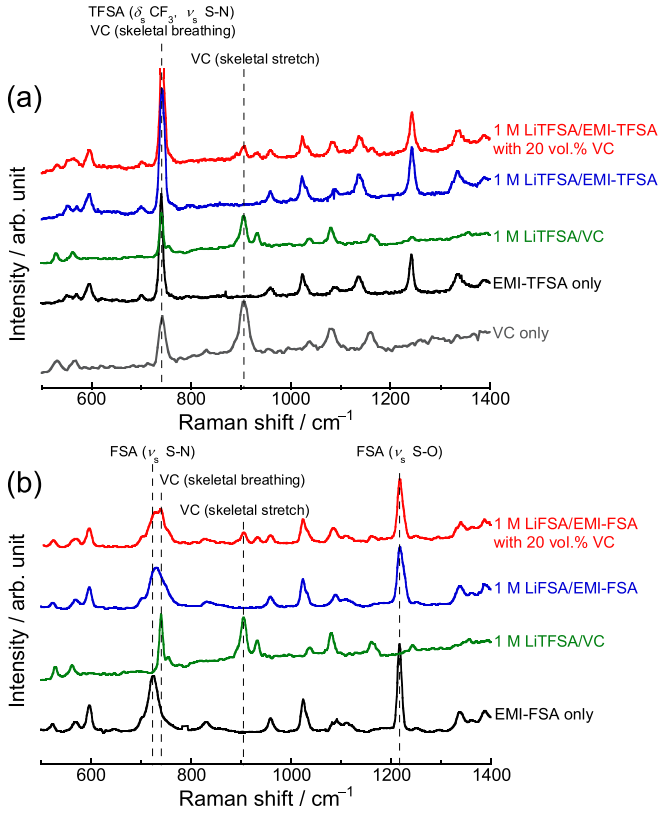

Figure 10. Raman spectra of (a) 1 M LiTFSA/EMI-TFSA and (b) 1 M LiFSA/EMI-FSA without and with 20 vol.% VC. For comparison, spectrum of 1 M LiTFSA/VC, VC, EMI-TFSA, and EMI-FSA was also shown in this figure.

1500 mA h g^{-1} cannot be obtained. In fact, capacity decay started at the 1150th cycle where cutoff potential reached 2.0 V in 1 M LiFSA/EMI-FSA. Thus, the discharge cutoff potential enables us to predict cycle life of the electrode. The cycle life in 1 M LiFSA/EMI-FSA with 20 vol.% VC can be much longer than that in the electrolyte without VC because its cutoff potential has stably maintained approximately 0.7 V over 1600 cycles. We demonstrated that VC addition is effective approach to enhance cycle life of Si electrode in FSA-based electrolyte also.

The electrolytes consisted of EMI-FSA have very high ionic conductivity, which is superior to electrolytes consisted of EMI-TFSA (Figure 9a and Table I). By adding VC to the electrolytes, the conductivity increased furthermore. Based on these conductivities, we expected that the combination of EMI-FSA with VC enable Si electrode to exhibit high rate capability beyond that in EMI-TFSA with VC. Figure 9b shows rate capability of Si electrode in the electrolyte consisted of EMI-FSA. Rate capability in 1 M LiFSA/EMI-FSA exceeded the performance in 1 M LiTFSA/EMI-TFSA with VC. For the combination of EMI-FSA with VC, higher performance was obtained: the electrode retained a discharge capacity of 2200 mA h g^{-1} and a capacity retention of 73% even at a current density of 4200 mA g^{-1} (1.2 *C*). It is noteworthy that this electrolyte can achieve such high rate capability without any structural design or surface modification of Si active material. We concluded that the combination of LiFSA/EMI-FSA with VC is one of the best electrolytes to enhance the cycling stability and rate capability of Si-based electrolyte.

Interaction of Li^+ and counter anion in ionic liquid.—We demonstrated that VC addition can increase the conductivity of EMI-based electrolyte. However, only increase in conductivity might be insufficient to explain the reason why rate capability of Si electrode is improved, because electrostatic interaction between Li^+ and counter anion in ionic liquid is too strong to cycle under high current density in general. Hardwick et al. reported that the electrostatic interaction between Li^+ and $TFSA^-$ is decreased by adding 2 M ethylene carbonate or VC to 0.5 M LiTFSA-dissolved EMI-TFSA.[43] Hence, we tried to elucidate the interaction between Li^+ and counter anion in the 20 vol.% VC-added electrolytes used in this study. Figure 10 shows Raman spectra of the electrolytes without and with VC. The intense bands were observed at 742 cm^{-1} in Figure 10a, which is attributed to the CF_3 bending vibration δ_s (CF_3) coupled with the S−N stretching vibration ν_s (S−N−S) of the TFSA anion.[44–46] It is well known that the band position of 742 cm^{-1} shifts to 748 cm^{-1} by coordination of TFSA anions to Li^+. Unfortunately, this band overlapped with Raman band at 742 cm^{-1} ascribed to skeletal breathing of VC,[47] complicating the peak deconvolution for analysis. On the other hand, in Figure 10b, the relatively intense bands were observed at 731 cm^{-1} and 1220 cm^{-1} attributed to the S−N stretching vibration ν_s (S−N) and the S−O stretching vibration ν_s (S−O) of the FSA anion without interaction (free FSA), respectively.[48] The band at 1220 cm^{-1} is also affected by coordination of FSA anions to Li^+ and does not overlap with VC-derived bands. Thus, we focused on the band at 1220 cm^{-1} to determine the effect of VC addition on the interaction between Li^+ and FSA^- anions.

Figure 11a shows the Raman spectra for the neat ionic liquid and the electrolyte containing LiFSA with/without VC in the wavenumber range of 1190 to 1250 cm^{-1}. Shoulder at around 1230 cm^{-1} was newly observed, which is ascribable to the FSA^- solvating to the Li^+ in ionic liquid (Li^+-FSA), regardless of the presence/absence of VC.[48] However, the intensity in the electrolyte with VC was slightly lower compared to that without VC. We conducted deconvolution of the

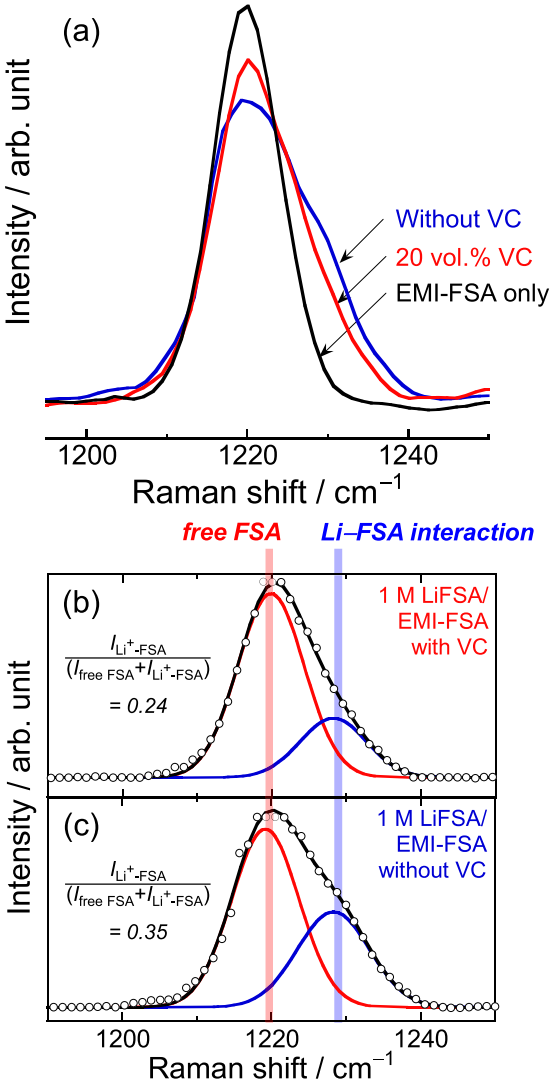

Figure 11 (a) Raman bands of neat EMI-FSA and the 1 M LiFSA/EMI-FSA with and without VC in the wavenumber range of 1190 to 1250 cm^{-1}. Deconvoluted Raman bands of 1 M LiFSA/EMI-FSA (b) with and (c) without 20 vol.% VC.

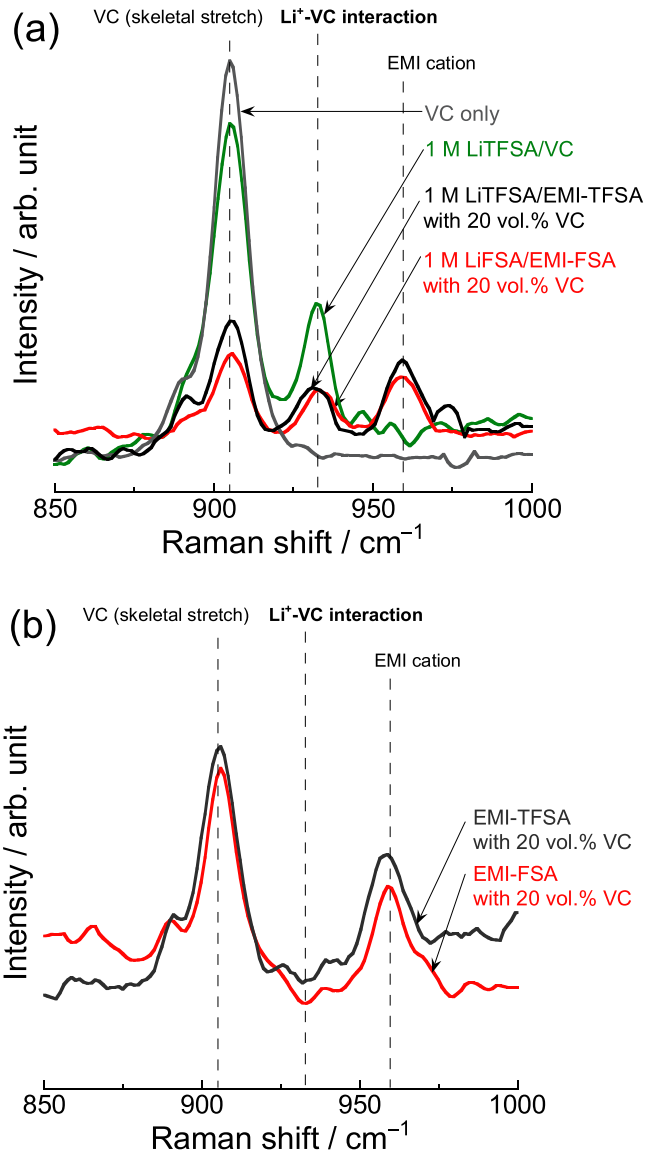

Figure 12. Raman spectra of (a) 1 M Li-salt-dissolved EMI-based electrolytes with 20 vol.% VC and (b) EMI-based ionic liquids with 20 vol.% VC in the wavenumber range of 850 to 1000 cm^{-1}.

Raman band, as shown in Figure 11b and 11c. The relative intensity derived from Li^+-FSA in the VC-added electrolyte was less than that in the VC-free electrolyte. The ratio of peak intensity of Li^+-FSA to sum intensity of Li^+-FSA and free FSA ($I_{Li+-FSA}/(I_{free\ FSA}+I_{Li+-FSA})$) was 0.35 in the electrolyte without VC. On the other hand, the ratio was 0.24 in the electrolyte with VC. This means that VC reduces the interaction of FSA^- with Li^+. Lower interaction leads to reduction of viscosity and high conductivity as well as smooth desolvation of FSA^- from Li^+. This tendency is presumably in the TFSA-based electrolyte also. In addition, VC can also solvate to Li^+ because of its high relative permittivity. The Raman band at 905 cm^{-1} corresponds to skeletal stretch of VC (free VC).[47] We confirmed that new Raman band appeared at around 930 cm^{-1} in 1 M LiTFSA/VC (Figure 12a). This Raman band was also observed in the EMI-based electrolytes with 20 vol.% VC, but did not appear in EMI-based ionic liquids (without Li salt) with 20 vol.% VC (Figure 12b). Therefore, this band should be attributed to the interaction between Li^+ and VC (Li^+-VC). We calculated the ratio of $I_{Li+-VC}/(I_{free\ VC}+I_{Li+-VC})$ and summarized in Table II. The ratio in the VC-added electrolytes was same or more than that in 1 M LiTFSA/VC. From this result, we propose that VC solvates Li^+. Since VC is electrically neutral unlike component of ionic liquids, the interaction between Li^+ and VC must be weaker compared to the electrostatic interaction between Li^+ and FSA^-/$TFSA^-$. The electrostatic interaction decreases with VC solvation, and desolvation process at the electrode–electrolyte interface can proceed smoothly. This is one of the reasons for achieving better cycling performance and rate capability.

Non-flammability estimation of VC-added electrolytes.—VC effectively exerted advantage of EMI-based ionic liquid electrolyte, and thus electrochemical performance of Si electrode significantly improved. However, the electrolytes contained not only ionic liquid

Table II. Ratio of peak intensity of Li^+-VC against sum intensity of Li^+-VC and free VC, namely $I_{Li+-VC}/(I_{free\ VC}+I_{Li+-VC})$ calculated by Figure 12a.

Electrolytes	$I_{Li+-VC}/(I_{free\ VC}+I_{Li+-VC})$
1 M LiTFSA/EMI-TFSA with 20 vol.% VC	0.30
1 M LiFSA/EMI-FSA with 20 vol.% VC	0.41
1 M LiTFSA/VC	0.29

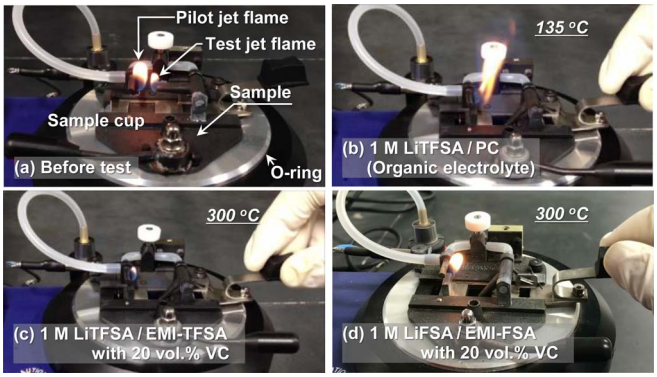

Figure 13. (a) Photographs of fire-resistance tester (Setaflash Series: 33000-0). Fire-resistance tests of (b) 1 M LiTFSA/PC (organic electrolyte), (c) 1 M LiTFSA/EMI-TFSA with 20 vol.% VC, and (d) 1 M LiFSA/EMI-FSA with 20 vol.% VC.

but also vinylene carbonate which is combustible, leading to fear to lose non-flammability of ionic liquid. Therefore, we evaluated non-flammability of the electrolytes with VC by using a flash point tester (Figure 13a). Generally, flammability evaluation of ionic liquid electrolytes has been examined by directly exposing it to a test flame at room temperature.[49,50] The vapor of the electrolyte generated by the heat hardly reaches its limit of inflammability because of an open-system measurement, though this test is a simple to easily understand. From this reason, the results have fear to be overestimated. On the other hand, the closed-system evaluation method (Rapid equilibrium closed cup method) used in this study is prescribed by ISO-standard and JIS. The flame retardant property can be evaluated with a good accuracy and reproducibility. We have introduced this technique as the evaluation method for non-flammability of ionic liquid electrolytes for the first time, and demonstrated its availability.[31,32] Figure 13b–13d shows fire resistance test results of the VC-added electrolytes. We also examined for 1 M LiTFSA/PC as a conventional organic electrolyte. The organic electrolyte ignited with a large flame at the relatively low temperature of 135°C (Figure 13b). In contrast, no fire was observed in both of 1 M LiTFSA/EMI-TFSA (Figure 13c) and 1 M LiFSA/EMI-FSA (Figure 13d) in spite of containing 20 vol.% VC even at 300°C which is measurement limit. The non-flammability of the VC-added ionic liquid electrolytes was clearly demonstrated by this method. From these results, we revealed that the EMI-based electrolyte with VC, especially 1 M LiFSA/EMI-FSA with 20 vol.% VC, is very promising in order to not only improve electrochemical performance of Si-based electrode but also to effectively increase safety of batteries.

Conclusions

In this study, we investigated the effect of adding VC as film-forming additive to EMI-based ionic liquid electrolytes on the electrochemical performance of Si-alone electrode for LIBs. The electrode exhibited an excellent cycling stability in 1 M LiFSA/EMI-FSA with 20 vol.% VC: a remarkably high capacity of 1500 mA h g^{-1} was maintained even after 1000 cycles, which was higher than that in EMI-TFSA-based electrolyte. This might be because the surface film derived from combination of FSA and VC is very stable during long-term cycling and suppresses the decomposition of EMI cation. An outstanding rate capability was also achieved in the electrolyte consisted of EMI-FSA and 20 vol.% VC. 1 M LiFSA/EMI-FSA with 20 vol.% VC had much higher conductivity of 18 mS cm^{-1} at 303 K compared to 1 M LiTFSA/EMI-TFSA with 20 vol.% VC. In addition, VC can solvate to Li^+ and reduce the electrochemical interaction between Li^+ and FSA. By achieving both of higher conductivity and smooth desolvation processes, outstanding rate capability can be obtained in VC-added electrolyte. Fire retardancy test revealed that non-flammability of EMI-based electrolyte was maintained even containing 20 vol.% VC until at least 300°C. Although the composition of surface film on the Si electrode was insufficiently understood (we will investigate in the near future), the combination of VC and EMI-based electrolyte (especially, EMI-FSA) must be one of the most promising candidate to enhance the cycling stability and rate capability of Si-based electrolyte as well as the safety of LIBs.

Acknowledgments

This work was partially supported by the Japan Society for the Promotion of Science (JSPS) KAKENHI (grant Numbers JP17H03128, JP16 K05954, and JP17 K17888).

ORCID

Hiroyuki Usui https://orcid.org/0000-0002-1156-0340
Masahiro Shimizu https://orcid.org/0000-0003-1084-7486
Hiroki Sakaguchi https://orcid.org/0000-0002-4125-7182

References

1. M. N. Obrovac and L. Christensen, *Electrochem. Solid-State Lett.*, **7**, A93 (2004).
2. J. Xie, N. Imanishi, T. Zhang, A. Hirano, Y. Takeda, O. Yamamoto, N. Ding, J. Xu, Y. X. Yao, G. Wegner, X. Fang, C. H. Chen, and I. Lieberwirth, *Mater. Chem. Phys.*, **120**, 421 (2010).
3. N. Ding, J. Xu, Y. X. Yao, G. Wegner, X. Fang, C. H. Chen, and I. Lieberwirth, *Solid State Ionics*, **180**, 222 (2009).
4. H. Sakaguchi, T. Iida, M. Itoh, N. Shibamura, and T. Hirono, *IOP Conf. Ser. Mater. Sci. Eng.*, **1**, 012030 (2009).
5. Y. Domi, H. Usui, Y. Takemoto, K. Yamaguchi, and H. Sakaguchi, *J. Phys. Chem. C*, **120**, 16333 (2016).
6. Y. Domi, H. Usui, M. Narita, Y. Fujita, K. Yamaguchi, and H. Sakaguchi, *J. Electrochem. Soc.*, **164**, A3208 (2017).
7. H. Usui, M. Nomura, H. Nishino, M. Kusatsu, T. Murota, and H. Sakaguchi, *Mater. Lett.*, **130**, 61 (2014).
8. S. Chou, J. Wang, J. Sun, D. Wexler, M. Forsyth, H. Liu, D. R. MacFarlane, and S. Dou, *Chem. Mater.*, **20**, 7044 (2008).
9. H. Tokuda, K. Hayamizu, K. Ishii, A. Susan, and M. Watanabe, *J. Phys. Chem. B*, **109**, 6103 (2005).
10. M. C. Buzzeo, C. Hardacre, and R. G. Compton, *ChemPhysChem*, **7**, 176 (2006).
11. S. P. Ong, O. Andreussi, Y. Wu, N. Marzari, and G. Ceder, *Chem. Mater.*, **23**, 2979 (2011).
12. H. Usui, T. Masuda, and H. Sakaguchi, *Chem. Lett.*, **41**, 521 (2012).
13. H. Usui, M. Shimizu, and H. Sakaguchi, *J. Power Sources*, **235**, 29 (2013).
14. M. Shimizu, H. Usui, K. Matsumoto, T. Nokami, T. Itoh, and H. Sakaguchi, *J. Electrochem. Soc.*, **161**, A1765 (2014).
15. K. Yamaguchi, Y. Domi, H. Usui, M. Shimizu, K. Matsumoto, T. Nokami, T. Itoh, and H. Sakaguchi, *J. Power Sources*, **338**, 103 (2017).
16. S. Tsuzuki, K. Hayamizu, and S. Seki, *J. Phys. Chem. B*, **114**, 16329 (2010).
17. A. A. Miran Beigi, M. Abdouss, M. Yousefi, S. M. Pourmortazavi, and A. Vahid, *J. Mol. Liq.*, **177**, 361 (2013).
18. H. Matsumoto, H. Sakaebe, K. Tatsumi, M. Kikuta, E. Ishiko, and M. Kono, *J. Power Sources*, **160**, 1308 (2006).
19. T. Sugimoto, M. Kikuta, E. Ishiko, M. Kono, and M. Ishikawa, *J. Power Sources*, **183**, 436 (2008).
20. T. Sugimoto, Y. Atsumi, M. Kono, M. Kikuta, E. Ishiko, M. Yamagata, and M. Ishikawa, *J. Power Sources*, **195**, 6153 (2010).
21. S. Hy, Y. H. Chen, H. M. Cheng, C. J. Pan, J. H. Cheng, J. Rick, and B. J. Hwang, *ACS Appl. Mater. Interfaces*, **7**, 13801 (2015).
22. S. K. Jeong, M. Inaba, R. Mogi, Y. Iriyama, T. Abe, and Z. Ogumi, *Langmuir*, **17**, 8281 (2001).
23. Y. Xiao, D. Hao, H. Chen, Z. Gong, and Y. Yang, *ACS Appl. Mater. Interfaces*, **5**, 1681 (2013).
24. V. Etacheri, O. Haik, Y. Goffer, G. A. Roberts, I. C. Stefan, R. Fasching, and D. Aurbach, *Langmuir*, **28**, 965 (2012).
25. D. Aurbach, K. Gamolsky, B. Markovsky, Y. Gofer, M. Schmidt, and U. Heider, *Electrochim. Acta*, **47**, 1423 (2002).
26. K. W. Schroder, J. Alvarado, T. A. Yersak, J. Li, N. Dudney, L. J. Webb, Y. S. Meng, and K. J. Stevenson, *Chem. Mater.*, **27**, 5531 (2015).
27. X. G. Sun and S. Dai, *Electrochim. Acta*, **55**, 4618 (2010).
28. T. Sugimoto, Y. Atsumi, N. Handa, M. Yamagata, M. Kono, M. Kikuta, E. Ishiko, and M. Ishikawa, *Electrochemistry*, **77**, 696 (2009).
29. D. M. Piper, T. Evans, K. Leung, T. Watkins, J. Olson, S. C. Kim, S. S. Han, V. Bhat, K. H. Oh, D. A. Buttry, and S.-H. Lee, *Nat. Commun.*, **6**, 1 (2015).
30. H. Sakaguchi, T. Toda, Y. Nagao, and T. Esaka, *Electrochem. Solid-State Lett.*, **10**, J146 (2007).
31. M. Shimizu, H. Usui, K. Yamane, T. Sakata, T. Nokami, T. Itoh, and H. Sakaguchi, *Int. J. Electrochem. Sci.*, **10**, 10132 (2015).
32. H. Usui, Y. Domi, M. Shimizu, A. Imoto, K. Yamaguchi, and H. Sakaguchi, *J. Power Sources*, **329**, 428 (2016).

33. M. Shimizu, H. Usui, T. Suzumura, and H. Sakaguchi, *J. Phys. Chem. C*, **119**, 2975 (2015).
34. G. G. Eshetu, T. Diemant, S. Grugeon, R. J. Behm, S. Laruelle, M. Armand, and S. Passerini, *ACS Appl. Mater. Interfaces*, **8**, 16087 (2016).
35. G. M. A. Girard, M. Hilder, N. Dupre, D. Guyomard, D. Nucciarone, K. Whitbread, S. Zavorine, M. Moser, M. Forsyth, D. R. MacFarlane, and P. C. Howlett, *ACS Appl. Mater. Interfaces*, **10**, 6719 (2018).
36. G. M. A. Girard, M. Hilder, D. Nucciarone, K. Whitbread, S. Zavorine, M. Moser, M. Forsyth, D. R. MacFarlane, and P. C. Howlett, *J. Phys. Chem. C*, **121**, 21087 (2017).
37. M. Nie, J. Demeaux, B. T. Young, D. R. Heskett, Y. Chen, A. Bose, J. C. Woicik, and B. L. Lucht, *J. Electrochem. Soc.*, **162**, A7008 (2015).
38. A. L. Michan, B. S. Parimalam, M. Leskes, R. N. Kerber, T. Yoon, C. P. Grey, and B. L. Lucht, *Chem. Mater.*, **28**, 8149 (2016).
39. Y. Jin, N. J. H. Kneusels, L. E. Marbella, E. Castillo-Martínez, P. C. M. M. Magusin, R. S. Weatherup, E. Jónsson, T. Liu, S. Paul, and C. P. Grey, *J. Am. Chem. Soc.*, **140**, 9854 (2018).
40. F. Lindgren, C. Xu, L. Niedzicki, M. Marcinek, T. Gustafsson, F. Björefors, K. Edström, and R. Younesi, *ACS Appl. Mater. Interfaces*, **8**, 15758 (2016).
41. K. Yamaguchi, Y. Domi, H. Usui, and H. Sakaguchi, *ChemElectroChem*, **4**, 3257 (2017).
42. Y. Domi, H. Usui, M. Shimizu, K. Miwa, and H. Sakaguchi, *Int. J. Electrochem. Sci.*, **10**, 9678 (2015).
43. L. J. Hardwick, M. Holzapfel, A. Wokaun, and P. Novák, *J. Raman Spectrosc.*, **38**, 110 (2007).
44. I. Rey, P. Johansson, J. Lindgren, J. C. Lassègues, J. Grondin, and L. Servant, *J. Phys. Chem. A*, **102**, 3249 (1998).
45. M. Herstedt, M. Smirnov, P. Johansson, M. Chami, J. Grondin, L. Servant, and J. C. Lassègues, *J. Raman Spectrosc.*, **36**, 762 (2005).
46. J. C. Lassègues, J. Grondin, R. Holomb, and P. Johansson, *J. Raman Spectrosc.*, **38**, 551 (2007).
47. J. R. Durig, J. W. Clark, and J. M. Casper, *J. Mol. Struct.*, **5**, 67 (1970).
48. K. Fujii, H. Hamano, H. Doi, X. Song, S. Tsuzuki, K. Hayamizu, S. Seki, Y. Kameda, K. Dokko, M. Watanabe, and Y. Umebayashi, *J. Phys. Chem. C*, **117**, 19314 (2013).
49. M. Montanino, M. Moreno, M. Carewska, G. Maresca, E. Simonetti, R. Lo Presti, F. Alessandrini, and G. B. Appetecchi, *J. Power Sources*, **269**, 608 (2014).
50. H. Nakagawa, Y. Fujino, S. Kozono, Y. Katayama, T. Nukuda, H. Sakaebe, H. Matsumoto, and K. Tatsumi, *J. Power Sources*, **174**, 1021 (2007).